이학석사 학위논문

Source change of surface water in the western Arctic Ocean recorded by neodymium isotopes since 76 kyr BP

네오디뮴 동위원소에 기록된 과거 76,000년간 서북극해로 유입된 표층수 변화 연구

2012년 08월

서울대학교 대학원

지구환경과학부 동위원소 지구화학연구실

장 광 철

Source change of surface water in the western Arctic Ocean recorded by neodymium isotopes since 76 kyr BP

지도 교수 허 영 숙

이 논문을 이학석사 학위논문으로 제출함
2012년 08월

서울대학교 대학원
지구환경과학부 동위원소 지구화학 연구실
장 광 철

장광철의 이학석사 학위논문을 인준함
2012년 08월

위 원 장 이 용 일 (인)

부위원장 허 영 숙 (인)

위 원 안 진 호 (인)

Abstract

Source change of surface water in the western Arctic Ocean recorded by neodymium isotopes since 76 kyr BP

Kwangchul Jang
Isotope Geochemistry Laboratory
School of Earth and Environmental Science
The Graduate School
Seoul National University

Keywords : neodymium isotope, western Arctic ocean, N. Pacific Ocean, surface water, freshwater, paleoclimate
Student Number : 2010-23138

The freshwater budget of the Arctic Ocean is an important component of the global climate system. Meltwater input, riverine discharge, and Pacific water inflow decrease the salinity of the Arctic Ocean and weaken the formation of the North Atlantic Deep Water (NADW) (Schlosser et al., 1991). Here I report continuous record of authigenic neodymium (Nd) isotopes on the Mendeleev Ridge from which I reconstruct prominent freshwater discharge events at 46-51, 35-39 and 13-19 ka BP. At 46-51 ka BP, there was freshwater input from bursting of ice-dammed lakes accompanying

the collapse of the Barent-Kara Ice Sheet during Middle Weichselian glaciation (Mangerud et al., 2004) releasing radiogenic Nd. The cyclonic surface circulation in the eastern Arctic Ocean was stronger than at present. At 35-39 and 13-19 ka BP, the Laurentide ice sheet (LIS) supplied freshwater which remobilized the unradiogenic Nd accumulated on the shelves. During both intervals the configuration of anticyclonic circulation in the western Arctic was expanded eastward or similar to today. Simple mass balance calculation suggests that 6,300, 10,600, and 4,800 km^3 of freshwater contributed these ε_{Nd} variations, implying that amount of freshwater could have also affected the formation of NADW. During late Holocene, the radiogenic trend toward the upper sediment layer imply that Pacific inflow to the Arctic Ocean was increased owing to sea-level rise. Two unradiogenic troughs were questionable due to lack of age and geochemical information.

Contents

Abstract

1. Introduction 1

2. Method 4

2.1. Sampling location 4

2.2. Nd isotope analysis 5

2.2.1. Fe-Mn hydroxide extraction 5

2.2.2. Column chemistry 7

2.2.3. TIMS analysis 8

3. Results and discussion 9

3.1. PS72/410-1 in the central Mendeleev Ridge 9

3.1.1. Core information 9

3.1.2. Age model 10

3.1.3. Nd isotopes 14

3.1.3.1. Radiogenic Nd record at 46-51 ka BP 14

3.1.3.2. Unradiogenic Nd records at 35-39 and 13-19 ka BP 16

3.1.3.3. Comparison with the Quaternary Lomonosov Ridge record 18

3.1.3.4. Mass balance 19

3.2. ARA02B/03B in the Chukchi Plateau 21

4. Conclusion 21

References 24

국문초록 48

Tables

[Table 1] 34
[Table 2] 35
[Table 3] 36
[Table 4] 37
[Table 5] 38

Figures

[Figure 1] 39
[Figure 2] 40
[Figure 3] 41
[Figure 4] 42
[Figure 5] 43
[Figure 6] 44
[Figure 7] 45
[Figure 8] 46
[Figure 9] 47

1. Introduction

The formation and melting of ice covering Arctic regions affect the variations in the albedo and freshwater budget of the Arctic Ocean and global eustatic sea level. Less saline Pacific inflow through shallow Bering Strait and high amounts of riverine discharge amplify the freshwater contents in the Arctic Ocean. As this freshwater directly flows to the North Atlantic through the Fram Strait and the Canadian Archipelago, the enhanced freshwater fluxes to the Arctic Ocean originate the salt deficit in the Atlantic and results in weakening of the formation of the North Atlantic Deep Water (NADW) (Peterson et al., 2002; Tarasov and Peltier, 2005). The Great Salinity Anomaly in the North Atlantic during in 1968-1982 (Dickson et al., 1988) is a recent example of a salinity depletion event caused by freshwater discharge from the Arctic Ocean (Aagaard and Carmack, 1989) and it possibly triggered the reduction of NADW during in 1978-1982 (Schlosser et al., 1991).

To reconstruct the freshwater event, paired reduction in ^{18}O and ^{13}C in planktonic foraminifera or occurrence of ice rafted debris (IRD) have been used (Darby et al., 2002; Poore et al., 1999). The $\delta^{18}O$ distribution of Arctic surface waters is significantly affected by regional salinity variations due to semi-enclosed Arctic environment and various freshwater inflows to the Arctic Ocean. As a result, the freshwater influx including rivers, meltwater, meteoric water and Pacific water can be regarded as the major reason of oxygen isotope depletion recorded in the planktonic foraminifera in the Arctic Ocean (Cooper et al., 2005; Stein et al., 1994). On the other hand, $\delta^{13}C$ depletion can be interpreted in two different ways (i) reduced ventilation by

strong stratification related to high freshwater discharge (Nørgaard-Pedersen et al., 2003), or (ii) limited air-sea gas exchange due to solid ice cover (Charles et al., 1993; Spielhagen and Erlenkeuser, 1994). Although more complicated, $\delta^{13}C$ depletion, if accompanied by $\delta^{18}O$ depletion, is interpreted as stratified and less productive surface waters (Poore et al., 1999). However, these stable isotopes cannot pinpoint the source of the freshwater, and these stable isotope values could be muted in the low sedimentation rate area such as central Arctic because surface water in the Arctic is rapidly restored to normal condition. The abrupt increase in IRD also represents freshwater inflow by melting of ice sheet (Darby et al., 2002), but it may not record events related to outburst of ice dammed lakes or events in distal areas.

The variation in the water mass including a significant input of the freshwater can be traced by neodymium (Nd) isotope ratios (expressed as $\varepsilon_{Nd} = [(^{143}Nd/^{144}Nd)_{sample}/(^{143}Nd/^{144}Nd)_{CHUR} - 1] \times 10^4$, where $(^{143}Nd/^{144}Nd)_{CHUR}$ is 0.512638 from Jacobsen and Wasserburg (1980)) extracted from the Fe-Mn oxyhydroxide fraction of marine sediments. Nd is preferentially concentrated in continental rocks while Sm tends to stay in mantle rocks because of the element compatibility (Faure and Mensing, 2005). Therefore, old continental crust has more negative ε_{Nd}, and young mantle rocks is more positive. Non-homogenous Nd characteristic in the ocean owing to short residence time of Nd (Tachikawa et al., 1999) allows the water mass to conserve specific Nd isotopes ratio in the source region without measurable fractionation and variable ^{143}Nd / ^{144}Nd value in the oceans are affected by the age and composition of the source rock (Piotrowski et al., 2009). Because these

distinct Nd isotope ratios are recorded in the Fe-Mn oxyhydroxide which precipitate upon the surface of biogenic and detrital materials from ambient water, Nd isotope ratios extracted from the Fe-Mn oxyhydroxide fraction of marine sediments reflect the water mass composition at the time of deposition (e.g. Frank et al., 2002; Piotrowski et al., 2009; Rutberg et al., 2000; Spivack and Wasserburg, 1988).

Surface water mass change in the Arctic Ocean is recorded in the entire water column. Basically, The water column of the Arctic Ocean is highly stratified, featuring the fresh Polar Mixed Layer at the surface, the cold Halocline Layer, the warm and saline Atlantic layer (AL) at approximately 200-850 m, the cooler and saltier Upper Polar Deep Water (UPDW) extending to 1,700 m, and the Polar Deep Water (PDW) (Porcelli et al., 2009). The average depth of the Lomonosov Ridge is 1,700 m and divides the PDW into the western Amerasian (subdivided into Canada and Makarov basins) and eastern Eurasian (subdivided into Amundsen and Nansen basins) basins. The PDW in the Eurasian Basin is derived mainly from the slope convection plume entraining water from the AL and UPDW, the cold and dense water formed in the Barents Sea, and from exchange with the Norwegian Sea Deep Water (Jones et al., 1995). The PDW in the Amerasian Basin is derived exclusively from density flow on the shelf, as exchange between the Makarov and Amundsen basins across the central Lomonosov Ridge is limited (Björk et al., 2007; Timmermans and Garrett, 2006). Consequently, the archives of PDW in the Canada Basin can track variation in surface freshwater input if changes in AL and UPDW can be determined independently or be ignored.

At present, the dissolved ε_{Nd} of PDW in the Canada Basin (-11.0 ± 0.4) is similar to that in the Makarov Basin (-10.5 ± 0.4, -10.7 ± 0.4) but different from that in the Amundsen Basin (-12.3 ± 0.4) (Porcelli et al., 2009). The AL display significant differences in dissolved ε_{Nd} in the four sub-basins (Porcelli et al., 2009). I infer that local slope convection affects the entire water column – AL, UPDW, and PDW – and gives rise to these basin-specific ε_{Nd} values.

Sediment core samples were obtained from two sampling area - the PS72/410 (Lat. 80°30.37′ N, Long. 175°44.38′ W, 1808 m water depth) in the central Mendeleev Ridge for long-term study during RV Polarstern Expedition ARK-23/3 in 2008 and the ARA02B/03B (Lat. 75°06.96′ N, Long. 166°20.31′ W, 453 m water depth) for high resolution study during ARAON Arctic Expedition 2011 (Fig. 1). I reconstructed the variation in the PDW and AL composition using authigenic Nd isotopes, and the contributions of surface water to the AL and PDW are identified by characteristic ε_{Nd} values. In the Arctic Ocean, the Atlantic water (-10.8), Mackenzie River (-13), and Lena River (-14) are possible unradiogenic water source while the Pacific water (-5), Kolyma River (-6), Ob River (-6) and Yenisey rivers (-5) are radiogenic (Fig. 1) (Porcelli et al., 2009).

2. Methods

2.1. Sampling locations

The sampling site PS72/410 and ARA02B/03B are shown in Fig. 1.

The 39 cm long sediment core 410-1 and 37.5 cm long sediment core ARA02B/03B was taken using the Giant Box Corer (GKG) and sampled onboard at 1 cm resolution. Because the present surface water current in the two sampling area is governed by Beaufort Gyre, the present surface water in the two sites are mainly affected by the Pacific inflow and Mackenzie River. However, the situation might be different at the past.

The past surface ocean circulation in the Arctic investigated using mineralogical composition of ice rafted debris (IRD) and inorganic and organic carbon content of sediments (Phillips and Grantz, 2001; Rella and Uchida, 2011) revealed that the western Arctic surface water has been mainly governed by the relative strengths of the Beaufort Gyre and the eastern Arctic by the Transpolar Drift since at least 650,000 years ago (Polyak and Jakobsson, 2011) and that the boundary between them has been variable (Rella and Uchida, 2011). For this reason, the record in the PS72/410-1 and ARA02B/03B might be affected by surface water inflow from the eastern Arctic Ocean.

2.2. Nd isotope analysis

2.2.1. Fe-Mn hydroxide extraction

The extraction of authigenic neodymium was accomplished by sequential chemical steps modified from Bayon et al. (2002), Chester and Hughes (1967) and Gutjahr et al. (2007).

Samples were freeze-dried at -55℃ and crushed gently in an agate

mortar. Mortar and pestle were washed with UP water and acetone and dried under heat lamp between each grinding steps. Quartz grains were ground in between sample to reduce cross-contamination.

About 1g of ground sediments were transferred to 15 ml centrifuge tube. To remove carbonate from the sediments, 10 ml of 1 M buffered acetic acid (pH ~5) was added to the centrifuge tube, which was filled up to ~14 ml after letting CO_2 escape from centrifuge tube. Samples were thoroughly mixed using a vortex mixer and agitated on a shaking table at room temperature for 12 hours. After centrifuging at 4,000 rpm for 15 minutes, the leachate composed of buffered acetic acid and dissolved carbonate was poured out to waste. The carbonate leaching step was repeated until carbonate was completely removed and no bubbles were visible. For most samples, 2 times would suffice.

The solid residue was disaggregated by vortex mixer or hand shaking, and rinsed with 14 ml of UP-water. Although the high centrifuge speeds make sediments harden, it reduces the chance of discarding the fine fraction with the leachate. The rinsing step was repeated until the color of the solution turned to yellowish brown which indicate colloid was suspended in the leachate because there was no acetic acid and dissolved carbonate. To aggregate the colloids, a few drops of buffered acetic acid were added, and the solution was centrifuged at 4,000 rpm for 5 minutes and discarded.

Fe-Mn hydroxide fraction was extracted using 13 ml 0.02 M hydroxylamine hydrochloride in 25% acetic acid on the decarbonated sediment. It was buffered to pH ~4 using ammonium hydroxide. After

sufficient mixing, the solution was agitated for 3 hours at room temperature. Although this mild leaching technique is not enough to extract all Fe-Mn hydroxides from the decarbonated sediments, it prevents Fe-Mn leachate from contamination by detrital phases.

After centrifuging at 4,000 rpm for 15 minute, the supernatant was transferred to a teflon beaker, and 1 ml of concentrated HNO_3 was added in order to remove excess reducing agent before evaporation. Finally, the sample was evaporated to dryness and stored in 0.5 ml of 2 M HNO_3.

2.2.2. Column chemistry

The following column separation method is modified from Míková and Denková (2007) and Pin and Zalduegui (1997).

Bio-rad Poly-Prep Chromatography Columns (0.8 cm ID, 5 cm long, and 10 ml reservoir) and TRU resin (50-100 μm, Eichrom) were used to separate LREEs from the extracted Fe-Mn hydroxide fraction. A slurry mixture of the TRU resin and 2.7 M HCl was packed to 0.25 ml bed of column, washed with 8 ml of UP-water, and pre-conditioned with 6 ml of 2 M HNO_3. The samples dissolved in 0.5 ml of 2 M HNO_3 were carefully poured into columns. After sample loading, Sr, Fe, Ca, HREEs were eluted with 8 ml of 2 M HNO_3. LREEs including neodymium were recovered using 6 ml of 0.05 M HCl. After each sample, the TRU resin was discarded because the working capacity of the resin was exceeded.

The LN resin (50-100 μm, Eichrom) was packed into columns which were made with heat shrinkable tubing (4:1 heat shrink, 1/2 in. minimum

expanded ID). The tubing was heated at 400 ℃ for approximately 1 minute with a well-fitted pyrex tube inserted to maintain the reservoir part from shrinking. The final columns were 3.66 mm ID, 6.5 cm long, and the reservoir size was 7 ml. The mixed slurry of LN resin and 6 M HCl was packed to a column bed of 0.7 ml. Fully packing was required to prevent air bubbles which disturb eluent flow. The column was washed with 12 ml of 6 M HCl followed by a pre-conditioning step with 6 ml of 0.05 M HCl. The samples from the TRU-resin were loaded on to the column. Matrix such as La, Ce, and Pr were eluted with 2 ml of 0.25M HCl and discarded. The neodymium fraction was collected in a cleaned teflon beaker by 5 ml of 0.25M HCl and evaporated to dryness. Unlike the TRU resin, the LN resin could be reused repeatedly without Nd blank problems. According to Míková and Denková (2007), however, periodic check is needed because elution interval might shift with used LN resin. As a result, ~200 ng of neodymium was obtained for mass spectrometry.

2.2.3. TIMS analysis

Nd isotopes were analyzed using IsotopX IsoProbe-T thermal ionization mass spectrometer at the Korea Basic Science Institute. Samples and standards were transferred onto Re outer filaments. The electric current applying heat to filaments was increased continuously, and it quickly dropped to zero after the most appropriate filament current which allows the best ion beams was maintained for 5 seconds. During this period, the best condition for analysis of neodymium isotope ratio was attained. The $^{147}Sm/^{146}Nd$ and

$^{146}Nd/^{144}Nd$ were analyzed for interference correction and mass fractionation, respectively. Data were normalized to daily variations of the standard JNdi-1 (0.512100 ± 0.000014, 2σ external reproducibility, n=109 for PS72/410-1 and 0.512105 ± 0.000017, 2σ external reproducibility for ARA02B/03B, n=19).

3. Results and discussions

3.1. PS72/410-1 in the central Mendeleev Ridge

3.1.1. Core information

The core is mainly composed of sandy-silty clay of brown to dark brown, dark yellowish brown, olive to olive brown, and dark grayish brown colors (Jokat, 2009; Stein et al., 2010) (Fig. 2). The surface is dark brown sandy mud with many dropstones (ø up to 2 cm). A cyclic alternation of brown to gray sediment was observed. It was probably caused by variations in manganese concentrations (Jakobsson et al., 2000) and is generally used as an indicator of interglacial (interstadial, high Mn) to glacial (stadial, low Mn) conditions (März et al., 2011). I classified sediment layers based on grain size and sediment color – L* (black to white) and a* (green to red) values (Table 1 and Fig. 2; data from Jang et al., *in preparation*). The B1 layer (0-4.5 cm) is characterized by dark brown sandy silty clay with relatively low L* and high a* values. These criteria for the brown layers are consistent with Adler et al. (2009) . The G1 layer (5.5-10 cm) was designated based on shipboard core description[6]. It was mainly composed of dark grayish brown clay to very dark grayish brown sandy silty clay. There is a condensed section

(CS) (10.5-14 cm) (see Age model section) of mainly brown silty clay. A thin layer of coarse material at the bottom of this section (13~14 cm) was also observed in neighboring cores 94B16 (80°20.33'N, 178°42.71'W; Poore et al., 1999) and HLY0503-8JPC (79°35.6′ N, 172°30.1′ W; (Adler et al., 2009; Polyak et al., 2009) on the Mendeleev Ridge. The B2 layer (14-20 cm) consisted of brown, dark brown, and dark yellowish brown silty clay with variable degrees of bioturbation. It had low L* and high a* values. White dolomite lenses and spots observed towards the top of the B2 layer is designated as the W3 layer (14-16 cm). The W3 layer was also identified in other neighboring Mendeleev Ridge cores (Adler et al., 2009; Polyak et al., 2009; Polyak et al., 2004) and I used it as a consistency check for my age model. Dolomite has been generally considered to derive from the Banks and Victoria islands in the Canadian Archipelago (Adler et al., 2009; Stein et al., 2010). The G2 layer (20-31 cm) contained dark grayish brown and olive brown silty clay. The B3 layer (32-39 cm) was similar to the B2 layer except for the larger grain size. In particular, a prominent ice rafted debris (IRD, > 2 mm) peak was observed at 33-34 cm. Some 'pinkish' spots were identified (36-39 cm), which is also consistent with previous descriptions of the B3 layer in other Mendeleev Ridge cores (Adler et al., 2009; Stein et al., 2010)

3.1.2. Age model

It has been difficult to construct age models for Arctic Ocean sediments because of the low sedimentation rates and limited biotic remains (Polyak et al., 2004). In recent years, several studies have used stratigraphic approaches

that brought together different proxies such as grain size, manganese content, total planktonic and benthic foraminiferal abundances, calcareous nannofossil abundances, lithology, L*, and $\delta^{18}O$ and $\delta^{13}C$ of planktonic foraminifera (Adler et al., 2009; Backman et al., 2009; Darby et al., 2006; Polyak et al., 2004). I used AMS ^{14}C ages (n=4) and correlated planktonic $\delta^{18}O$ and $\delta^{13}C$ with cores 94B16 and HLY0503-8JPC on the Mendeleev Ridge (Fig. 3). To extend the age model beyond the range of ^{14}C, I also used L* values and sediment lithology. Because planktonic $\delta^{18}O$ and $\delta^{13}C$ signals in the Arctic Ocean are governed more by the local environment than by global temperature or ice volume changes, I expect that correlations with neighboring cores should be meaningful if other age constraints are used in combination.

AMS ^{14}C ages were obtained for planktonic foraminifera (*N. pachyderma* sin.) at depth intervals 1-2 cm, 10-11 cm, 13-14 cm, and 20-21cm at Leibniz Laboratory, Kiel and converted to calendar years using Marine09 (Reimer et al., 2009) to ca. 5.1 ka, 19.8 ka, 30.8 ka and 45.8 ka BP, respectively (Table 2; data from Jang et al., *in preparation*). A regional difference of reservoir effect ($\triangle R$ = 1,000) was assumed(Hanslik et al., 2010). I also recalculated the AMS ^{14}C ages of cores 94B16, HLY0503-8JPC, and PS2185 to avoid treatment bias (Table 2).

Based on these calibrated ^{14}C ages, I used $\delta^{18}O$ and $\delta^{13}C$ of planktonic foraminifera (*N. pachyderma* sin.)(data from Jang et al., *in preparation*) for stratigraphic correlation with cores 94B16 and HLY0503-8JPC for which age models already exist (Adler et al., 2009; Poore et al., 1999). Six $\delta^{18}O$ and $\delta^{13}C$

tie points were matched to core 94B16, and two of them were used as age control points (Fig. 3). All tie points were well correlated between the two cores without any age reversal problem. Strongly reduced sedimentation rates were recorded in the 10-14 cm interval of core PS72/410-1, which has been interpreted to be either a hiatus (Polyak et al., 2009) or removal of sediments deposited during Marine Isotope Stage (MIS) 2 by contour currents (Poore et al., 1999). The bioturbated nature and absence of an unconformity in the x-radiograph deter a rigorous interpretation for this interval. This condensed section (CS) is bracketed by AMS ages in 94B16 and has an AMS age at its base in PS72/410-1, suggesting that it lasted from 30.8 ka BP to 12.7 ka BP. The AMS ^{14}C age for termination of the CS in core PS72/410-1 (19.8 ka BP at 10.5 cm) (Table 2) is older than the 12.7 ka BP termination age and is probably due to contamination by melt water derived from northwest Canada containing old carbon or from poor preservation of pristine foraminifera in the CS.

Cores PS72/410-1 and HLY0503-8JPC were correlated using eight $\delta^{18}O$ and $\delta^{13}C$ tie points based on age constraints including L* and sediment color (Fig. 3). The ages of the youngest six tie points roughly agree with those observed in both 94B16 and PS72/410-1. In core HLY0503-8JPC the top of the CS is interpolated to an age of 13 ka BP. Thus, considering all three cores, the age of the CS may be regarded as 12.7-30.8 ka BP.

Two of the eight stable isotope tie points between core PS72/410-1 and HLY0503-8JPC were used as age control points (Fig. 3). Light $\delta^{18}O$ and $\delta^{13}C$ at 26.5 cm depth in PS72/410-1 were also observed at >50 ka in core 94B16

and at 51.1 ka BP in core HLY0503-8JPC. I used this age (51.1 ka BP) to constrain the age model for PS72/410-1. The age control point of heavy $\delta^{18}O$ and light $\delta^{13}C$ at 31.5 cm depth in PS72/410-1 (Adler et al., 2009; Spielhagen et al., 2004) was also a prominent feature observed in the other two cores.

I also correlated stratigraphic sequences including brown layers B1 to B3, and white layer W3 (Fig. 3). The base of B1 marks 8.4 ka BP, which is consistent within the AMS age framework of the three cores. The AMS age of 45.8 ka BP at 20.5 cm slightly below the base of B2 in PS72/410-1, the 44.6 ka at 26.5 cm in the B2 layer of 94B16, and the 41.3 and 43.3 ka BP at 56.5 cm and 62.5 cm in the B2 layer of HLY0503-8JPC agree fairly well. The age of the B3 layer in PS72/410-1 can be constrained by that in HLY0503-8JPC based on the B. aculeate event and is consistent with the age obtained using planktonic $\delta^{18}O$ and $\delta^{13}C$ and L*. In particular, the initiation (75.7 ka BP) and termination (74.2 ka BP) ages of the B3 layer in HLY0503-8JPC were tentatively applied to the age of the B3 layer in PS72/410-1. The age of the W3 layer at 14-16 cm is comparable to those determined in other Mendeleev Ridge cores.

In summary, I used three calibrated AMS ^{14}C ages, four stable isotope correlation ages (two from 94B16 and two from HLY0503-8JPC), and two stratigraphic ages (the initiation and termination of the B3 layer). According to my tentative age model for PS72/410-1 which extends to MIS 5a (Fig. 4), the sedimentation rates during interstadial periods were generally higher than during stadial periods.

3.1.3. Nd isotopes

The core top ε_{Nd} was -10.63 ± 0.27 (2σ) which is similar to that of the present-day water column in the Canada Basin at 1000 and 3000 m depths (Porcelli et al., 2009) and gave assurance that authigenic ε_{Nd} reflects the seawater composition (Fig. 5, Table 3). The average ε_{Nd} (n=39) throughout the sampled period was -10.2 ± 1.7 (2σ), similar to the core top value, from which three periods of significant ε_{Nd} deviations occurred.

3.1.3.1. Radiogenic Nd record at 46~51 ka BP

Pronounced ε_{Nd} high was observed at 46-51 ka BP. It followed the minima in $\delta^{18}O$ and $\delta^{13}C$ of planktonic foraminifera (*N. pachyderma* sin.) at 51 ka BP (Fig. 5). I speculated that radiogenic ε_{Nd} at 46-51 ka BP was a consequence of episodic large input of radiogenic freshwater. The long lasting Nd peak relative to the $\delta^{18}O$ and $\delta^{13}C$ was caused by much longer residence time of the PDW than surface water (Macdonald and Bewers, 1996). The source of freshwater can be constrained based on the radiogenic ε_{Nd} to the Pacific inflow or the Kolyma, Yenisey or Ob rivers (Fig. 1). The only gateway to the Pacific, the Bering Strait, is narrow (~85 km), shallow (~50 m) and almost closed at ~50 ka BP (Hu et al., 2010), so I can rule out the Pacific Ocean.

The recent Nd flux from the Yenisey and Ob rivers into the Arctic Ocean, calculated by multiplying dissolved Nd concentrations by the annual river discharges (Porcelli et al., 2009 and references therein), were ~100 times greater than that from the Kolyma River (Table 4). This disparity is expected

to have been more extreme at ~50 ka BP. During the Middle Weichselian (60-50 ka BP), the ice sheet expanded from the Barents and Kara Sea shelves to west Siberia including mainland Russia (Svendsen et al., 2004), blocked northward riverine discharge of Yenisey and Ob rivers, and made ice dammed lakes in northern Eurasia(Mangerud et al., 2004). Estimated minimal proglacial lake volumes in the West Siberian Plain and White Sea Basin are 32,000 and 15,000 km^3, respectively (Mangerud et al., 2004). Furthermore, mechanical weathering of the Putoranan basalts (ε_{Nd} ~2; Sharma et al., 1992) under the ice sheet could provide more radiogenic Nd to the ice dammed lake during the Middle Weichselian (Fig. 1). The low inorganic carbon content at 46-51 ka BP is consistent with the carbonate poor Yenisey-Ob source area (Phillips and Grantz, 2001 and references therein)

For the radiogenic ε_{Nd} signals from the west Siberian shelf to be recorded in the Mendeleev Ridge, the cyclonic surface water circulation in the eastern Arctic must have extended to the Canada Basin (e.g. Rella and Uchida, 2011) and fed the PDW by brine formation possibly near the Chukchi Sea (Jones et al., 1995). Such surface circulation pattern is analogous to the present-day positive Arctic Oscillation (AO) mode (Morison et al., 2012). The past surface ocean circulation in the Arctic investigated using mineralogical composition of IRD and inorganic and organic carbon content of sediments (Phillips and Grantz, 2001; Rella and Uchida, 2011) revealed that the western Arctic surface water has been mainly governed by the relative strengths of the Beaufort Gyre and the Transpolar Drift since at least 650,000 years ago and that the boundary between them has been variable (Rella and Uchida, 2011).

The outburst of ice dammed lakes at ~50 ka, which released over 47,000 km^3 of fresh water (Mangerud et al., 2004), can be a reason of change in surface ocean circulation. This voluminous freshwater discharge would have led to the collapse of the NADW and rise of dynamic ocean topography in the North Atlantic (Levermann et al., 2005). The consequent flow reversal from the Atlantic to the Pacific would have enforced cyclonic surface circulation in the Arctic Ocean, the situation intensified by nearly closed Bering Strait due to lack of outlet toward the Pacific (Hu et al., 2012). The cyclonic circulation would have invaded the western Arctic and the radiogenic eastern Arctic surface water descended into the western Arctic PDW by brine formation possibly near the Chukchi shelf area.

3.1.3.2. Unradiogenic Nd records at 35-39 and 13-19 ka BP

Prominent ε_{Nd} reductions at 35-39 ka BP and 13-19 ka BP were observed with the inorganic carbon contents which are higher than and comparable to that at the present, respectively (Fig. 5). It implies that the general configuration of the Beaufort Gyre was expanded toward the eastern Arctic or similar to today, and unradiogenic Nd mainly derived from western Arctic area. The unradiogenic Nd can be traced to the Precambrian Canadian Shield (Fig. 1) and the high inorganic carbon content to the extensive carbonate distribution in the Canadian Archipelago (Phillips and Grantz, 2001 and references therein). In particular, the white dolomite layer attributed to the Banks and Victoria islands (Stein et al., 2010) was also observed at 35-37 ka BP. From this, I infer that abrupt meltwater discharges from the waning LIS

on the Canadian Shield toward the Canadian Archipelago is responsible for the two unradiogenic ε_{Nd} excursions. High mechanical erosion under the LIS may have accumulated weathering products containing unradiogenic Nd on the exposed shelves. When the LIS disintegrated, this material interacted with the meltwater to release unradiogenic Nd to the Arctic surface waters. The coarse-grained (> 2 mm) IRD peaks follow the two unradiogenic ε_{Nd} excursions with a lag of a few thousand years (Fig. 5; data from Jang et al., *in preparation*), and it support the existence of LIS. Light $\delta^{18}O$ and $\delta^{13}C$ values during these time intervals were also observed, but less outstanding than previous event, again indicating freshwater input (Fig. 5). Muted $\delta^{18}O$ and $\delta^{13}C$ would be interpreted by lower sedimentation rate than 46-51 ka BP event (1/6 and 1/2, respectively), or reduced population of *N. pachyderma* during freshwater discharge events by saline habitat loss.

The much higher inorganic carbon content and occurrence of the dolomitic white layer at 35-37 BP ka and not at 13-19 ka BP implies that the pathways of LIS meltwater discharge from the LIS were different. The major direction of meltwater and icebergs were that of the M'Clure Strait ice stream passing by the Banks and Victoria islands (Stokes et al., 2006; Stokes et al., 2005) at 35-39 ka BP and the Mackenzie ice stream (Winsborrow et al., 2004) at 13-19 ka BP (Fig. 1). In particular, the youngest event might be related to the outburst of Lake Agassiz to the Arctic during the Younger Dryas (Not and Hillaire-Marcel, 2012) which intensified the flux of unradiogenic Nd to the Arctic Ocean. However, it is open debate due to no data point between 13 and 19 ka BP.

3.1.3.3. Comparison with the Quaternary Lomonosov Ridge record

During slope convection to form the PDW, the descending surface water can entrain significant amounts of water from the Atlantic Layer (AL; 200 ~ 850 m, Porcelli et al., 2009) and the Upper Polar Deep Water (UPDW; 850 ~ 1,700 m, Porcelli et al., 2009). In order to evaluate the influences of the UPDW, I compared my data with core PS2185 (87.5° N, 144.4° E, 1,074 m water depth) on the Lomonosov Ridge (Haley et al., 2007) (Figs. 1 and 6). This comparison is reasonable as the AL and UPDW generated in the eastern Arctic Ocean are distributed to the western Arctic Ocean (Woodgate et al., 2001).

The Lomonosov Ridge record is of lower resolution than my Mendeleev Ridge record, but the average ε_{Nd} values are similar between the two records and with the average AL value (Porcelli et al., 2009). In the 55-76 ka BP period, radiogenic ε_{Nd} is only observed in the Lomonosov Ridge record (Fig. 6).It infer that there was input of radiogenic Nd to surface waters which was localized in the eastern Arctic and fed the UPDW there. It could be that (i) the UPDW of the eastern Arctic is distributed to the western Arctic but negligible amounts are incorporated into the sinking brine locally or (ii) that the UPDW in the Canada Basin is isolated from the eastern Arctic and mainly affected by local surface water as is the case for the PDW. In either case, the UPDW in the eastern Arctic is not a significant source for the PDW of the Canada Basin. Outburst of the ice-dammed lake changed the situation at 46-51 ka BP, and the surface waters of the eastern Arctic expanded to the west and affected its PDW. At this time, radiogenic ε_{Nd} is observed in both the

Lomonosov and Mendeleev ridge records. At 30-40 ka BP, collapse of the LIS released unradiogenic Nd to the western Arctic surface waters which affected its PDW but its influence was contained to the western Arctic by the Beaufort Gyre. The unradiogenic ε_{Nd} is only observed in the Mendeleev Ridge record.

3.1.3.4. Mass balance

I calculated using a simple mass balance model how much meltwater is necessary to give rise to the three ε_{Nd} excursions (Fig. 7). I took the ε_{Nd} value (-10.63) of the core top and present-day Nd concentration of PDW (16.7 pM) (Porcelli et al., 2009) as the PDW end member. The volume of PDW in the Amerasian Basin was assumed to be 4×10^6 km^3 (note that the volume of water mass deeper than 1,700 m in the central Arctic basin is ~5.27×10^6 km^3; Jakobsson (2002)). The freshwater end member for the 46-51 ka BP was the Putoranan basalt (ε_{Nd} = +2 from Sharma et al., (1992)), and that for the 35-39 ka BP and 13-19 ka BP was the Canadian Shield (ε_{Nd} = -24 from Winter et al., (1997)). The Nd concentration for the radiogenic end member was assigned a value (2,000 pM) similar to the present day Ob River draining the Putoranan Plateau (Zimmermann et al., 2009). For the unradiogenic end member a lower concentration was assigned (1,000 pM) because present day Mackenzie River draining the Canadian Shield has much lower concentrations, on the order of a few hundred pM (Zimmermann et al., 2009). It is likely that the high mechanical erosion under glacial conditions supplied more dissolved Nd to the ice dammed lakes and deposited more particulate Nd on the exposed shelves to be remobilized by abrupt freshwater discharge events. Thus, my Nd

concentrations for these freshwater endmembers are underestimates. According to the mass balance calculation, the freshwater added to the PDW in the western Arctic were 6,300 km^3 at 46-51 ka BP, 10,600 km^3 at 35-39 ka BP, and 4,800 km^3 at 13-19 ka BP.

For the 45-51 ka BP event, the source of freshwater was in the eastern Arctic which made its way into the western Arctic surface water and eventually into western Arctic PDW. If I assume for that event that equal amounts of surface water sank to PDW in the western and in the eastern Arctic Ocean, the freshwater input to PDW of the whole Arctic was 12,600 km^3. As the total volume released by ice dammed lakes is estimated to be 50,000 km^3 at that time (Mangerud et al., 2004), this means that a quarter was removed to PDW in the whole Arctic Ocean (Fig. 8). Extrapolating this rate of formation of PDW, the volume of meltwater discharges at 35-39 ka BP and at 13-19 ka BP would have been four times what sank to PDW in the western Arctic – 42,400 km^3 and 19,200 km^3, respectively (Fig. 8). The estimated meltwater discharge for the 13-19 ka BP is twice what has been appraised for glacial lake Agassiz (Leverington et al., 2000). The discrepancy may be due to problems with my initial assumptions. First, PDW formation rate may have been more active during the 35-39 ka BP and 13-19 ka BP than during the 46-51 ka BP. Second, I may have underestimated the Nd concentration for the freshwater endmembers. Note that the surface water transfer from the western to the eastern is assumed to be negligible for the two unradiogenic ε_{Nd} periods because of the Beaufort Gyre (Fig. 8).

3.2. ARA02B/03B in the Chukchi Plateau

The core top ε_{Nd} was -7.17 ± 0.34 (2σ) which is more radiogenic than recent AL values in the Canada Basin (Porcelli et al., 2009)(Fig. 9, Table 5). It implies that the AL composition in the Chukchi Plateau could be strongly affected by radiogenic Pacific inflows. The average ε_{Nd} (n=18) was -7.3 ± 1.3 (2σ) and there is an increase trend of ε_{Nd} values toward upper layer of sediment core. Although the lack of foraminifera and stratigraphic markers could not provide accurate ages of ARA02B/03B core, tentative age model based on the sedimentation rate of neighboring core imply that the age extends late Holocene (Nam per. communication). According to Hu et al. (2010), the melting of ice sheet during deglacial period generated sea level rise and reopening of shallow Bering Strait. Consequent increase in the Pacific inflow could be main reason of radiogenic ε_{Nd} trend toward recent period.

The unradiogenic troughs were also observed at the 17-18 cm and 28-29 cm (Fig. 9). Possible reason of them is an increase in the Mackenzie River inflow, meltwater discharge from LIS, or short period glacial event which prevents the Pacific inflow. To verify these hypotheses, age model construction and geochemical data such as $\delta^{18}O$ and $\delta^{13}O$ values are requested.

4. Conclusion

From measurements of authigenic neodymium isotopes from marine sediment on the Canada Basin side of central Mendeleev Ridge and Chucki

Plateau, I could reconstruct the variation in the Arctic surface water.

There were three prominent neodymium peaks at 46-51, 35-39, and 13-19 ka BP in the PS72/410-1. All peaks are consistent with planktonic $\delta^{18}O$ and $\delta^{13}C$ depletion and this correspondence indicate that deviations of ε_{Nd} value result from fresh water. The radiogenic ε_{Nd} peak accompanied by low carbonate contents at ~50 ka represents that the outburst of ice-dammed lakes from western Siberia as a consequence of the Middle Weichselian deglaciation could have affected the PDW in the western Arctic Ocean. On the contrary, the unradiogenic ε_{Nd} troughs coincided with an increase in carbonate contents indicate that the meltwater discharge from Laurentide Ice Sheet was mainly responsible. These fresh waters seemed to contain high amount of weathering product by two major glaciations, and they probably influenced the PDW by slope convection triggered by brine formation.

The freshwater input to the surface layer would have been larger at 46-51, 35-39, and 13-19 ka BP, and as the Arctic surface water directly feeds the North Atlantic, it would have disturbed the formation of NADW and induced abrupt changes in climate. The freshwater pulses recorded by authigenic neodymium isotopes concur in general with the weakening of the NADW formation as indicated by $\delta^{13}C$ records of benthic foraminifera *Cibicides wuellerstorfi* and with the IRD occurrences (Elliot et al., 2002). However, age uncertainty and sample resolution do not allow us to evaluate this hypothesis rigorously.

ARA02B/03B record suggested that the Pacific inflow were increased during late Holocene and short-period deglacial events related to the

meltwater discharge or glacial events related to the sea level drop might be occurred. Further researches would be essential to assess them.

References

Aagaard, K., Carmack, E.C., 1989. The role of sea ice and other fresh water in the Arctic circulation. J. Geophys. Res 94, 14485-14498.

Adler, R.E., Polyak, L., Ortiz, J.D., Kaufman, D.S., Channell, J.E.T., Xuan, C., Grottoli, A.G., Sellén, E., Crawford, K.A., 2009. Sediment record from the western Arctic Ocean with an improved Late Quaternary age resolution: HOTRAX core HLY0503-8JPC, Mendeleev Ridge. Global Planet. Change 68, 18-29.

Backman, J., Fornaciari, E., Rio, D., 2009. Biochronology and paleoceanography of late Pleistocene and Holocene calcareous nannofossil abundances across the Arctic Basin. Mar. Micropaleontol. 72, 86-98.

Bayon, G., German, C.R., Boella, R.M., Milton, J.A., Taylor, R.N., Nesbitt, R.W., 2002. An improved method for extracting marine sediment fractions and its application to Sr and Nd isotopic analysis. Chem. Geol. 187, 179-199.

Björk, G., Jakobsson, M., Rudels, B., Swift, J.H., Anderson, L., Darby, D.A., Backman, J., Coakley, B., Winsor, P., Polyak, L., Edwards, M., 2007. Bathymetry and deep-water exchange across the central Lomonosov Ridge at 88–89°N. Deep-Sea Res. Part I 54, 1197-1208.

Charles, C.D., Wright, J.D., Fairbanks, R.G., 1993. Thermodynamic influences on the marine carbon isotope record. Paleoceanography 8, 691-697.

Chester, R., Hughes, M.J., 1967. A chemical technique for the separation of ferro-manganese minerals, carbonate minerals and adsorbed trace elements from pelagic sediments. Chem. Geol. 2, 249-262.

Cooper, L.W., Benner, R., McClelland, J.W., Peterson, B.J., Holmes, R.M., Raymond, P.A., Hansell, D.A., Grebmeier, J.M., Codispoti, L.A., 2005. Linkages among runoff, dissolved organic carbon, and the stable oxygen isotope composition of seawater and other water mass indicators in the Arctic Ocean. J. Geophys. Res. 110.

Darby, D.A., Bischof, J.F., Spielhagen, R.F., Marshall, S.A., Herman, S.W., 2002. Arctic ice export events and their potential impact on global climate during the late Pleistocene. Paleoceanography 17, 15.11-15.17.

Darby, D.A., Polyak, L., Bauch, H.A., 2006. Past glacial and interglacial conditions in the Arctic Ocean and marginal seas—a review. Prog. Oceanogr. 71, 129-144.

Dickson, R.R., Meincke, J., Malmberg, S.-A., Lee, A.J., 1988. The "Great Salinity Anomaly" in the northern North Atlantic 1968-1982. Prog. Oceanogr. 20, 103-151.

Elliot, M., Labeyrie, L., Duplessy, J.C., 2002. Changes in North Atlantic deep-water formation associated with the Dansgaard-Oeschger temperature oscillations (60-10 ka). Quat. Sci. Rev. 21, 1153-1165.

Faure, G., Mensing, T.M., 2005. Isotopes: principles and applications. John Wiley & Sons Inc.

Frank, M., Whiteley, N., Kasten, S., Hein, J.R., O'Nions, K., 2002. North Atlantic Deep Water export to the Southern Ocean over the past 14

Myr: Evidence from Nd and Pb isotopes in ferromanganese crusts. Paleoceanography 17, 1022-1030.

Gutjahr, M., Frank, M., Stirling, C.H., Klemm, V., van de Flierdt, T., Halliday, A.N., 2007. Reliable extraction of a deepwater trace metal isotope signal from Fe-Mn oxyhydroxide coatings of marine sediments. Chem. Geol. 242, 351-370.

Haley, B.A., Frank, M., Spielhagen, R.F., Eisenhauer, A., 2007. Influence of brine formation on Arctic Ocean circulation over the past 15 million years. Nat. Geosci. 1, 68-72.

Hanslik, D., Jakobsson, M., Backman, J., Björck, S., Sellén, E., O'Regan, M., Fornaciari, E., Skog, G., 2010. Quaternary Arctic Ocean sea ice variations and radiocarbon reservoir age corrections. Quat. Sci. Rev. 29, 3430-3441.

Hu, A., Meehl, G.A., Han, W., Timmermann, A., Otto-Bliesner, B., Liu, Z., Washington, W.M., Large, W., Abe-Ouchi, A., Kimoto, M., 2012. Role of the Bering Strait on the hysteresis of the ocean conveyor belt circulation and glacial climate stability. Proc. Natl. Acad. Sci. U.S.A. 109, 6417-6422.

Hu, A., Meehl, G.A., Otto-Bliesner, B.L., Waelbroeck, C., Han, W., Loutre, M.F., Lambeck, K., Mitrovica, J.X., Rosenbloom, N., 2010. Influence of Bering Strait flow and North Atlantic circulation on glacial sea-level changes. Nat. Geosci. 3, 118-121.

Jacobsen, S.B., Wasserburg, G.J., 1980. Sm-Nd isotopic evolution of chondrites. Earth Planet. Sci. Lett. 50, 139-155.

Jakobsson, M., 2002. Hypsometry and volume of the Arctic Ocean and its constituent seas. Geochem. Geophys. Geosyst. 3, 1-18.

Jakobsson, M., Løvlie, R., Al-Hanbali, H., Arnold, E., Backman, J., Mörth, M., 2000. Manganese and color cycles in Arctic Ocean sediments constrain Pleistocene chronology. Geology 28, 23-26.

Jakobsson, M., Mayer, L., Coakley, B., Dowdeswell, J.A., Forbes, S., Fridman, B., Hodnesdal, H., Noormets, R., Pedersen, R., Rebesco, M., Schenke, H.W., Zarayskaya, Y., Accettella, D., Armstrong, A., Anderson, R.M., Bienhoff, P., Camerlenghi, A., Church, I., Edwards, M., Gardner, J.V., Hall, J.K., Hell, B., Hestvik, O., Kristoffersen, Y., Marcussen, C., Mohammad, R., Mosher, D., Nghiem, S.V., Pedrosa, M.T., Travaglini, P.G., Weatherall, P., 2012. The International Bathymetric Chart of the Arctic Ocean (IBCAO) Version 3.0. Geophys. Res. Lett. 39.

Jokat, W., 2009. The Expedition of the Research Vessel "Polarstern" to the Arctic in 2008 (ARK-XXIII/3). Reports on Polar and Marine Research, pp. 1-222.

Jones, E., Rudels, B., Anderson, L., 1995. Deep waters of the Arctic Ocean: origins and circulation. Deep-Sea Res. Part I 42, 737-760.

Leverington, D.W., Mann, J.D., Teller, J.T., 2000. Changes in the bathymetry and volume of glacial lake Agassiz between 11,000 and 9300 ^{14}C yr B.P. Quat. Res. 54, 174-181.

Levermann, A., Griesel, A., Hofmann, M., Montoya, M., Rahmstorf, S., 2005. Dynamic sea level changes following changes in the thermohaline circulation. Clim. Dyn. 24, 347-354.

Lisiecki, L.E., Raymo, M.E., 2005. A Plio-Pleistocene stack of 57 globally distributed benthic δ18O records. Paleoceanography 20.

Míková, J., Denková, P., 2007. Modified chromatographic separation scheme for Sr and Nd isotope analysis in geological silicate samples. J. Geosci. 52, 221-226.

März, C., Stratmann, A., Matthiessen, J., Meinhardt, A.K., Eckert, S., Schnetger, B., Vogt, C., Stein, R., Brumsack, H.J., 2011. Manganese-rich brown layers in Arctic Ocean sediments: Composition, formation mechanisms, and diagenetic overprint. Geochim. Cosmochim. Acta 75, 7668-7687.

Macdonald, R., Bewers, J., 1996. Contaminants in the arctic marine environment: priorities for protection. ICES J. Mar. Sci. 53, 537-563.

Mangerud, J., Jakobsson, M., Alexanderson, H., Astakhov, V., Clarke, G.K.C., Henriksen, M., Hjort, C., Krinner, G., Lunkka, J.-P., Möller, P., Murray, A., Nikolskaya, O., Saarnisto, M., Svendsen, J.I., 2004. Ice-dammed lakes and rerouting of the drainage of northern Eurasia during the Last Glaciation. Quat. Sci. Rev. 23, 1313-1332.

Morison, J., Kwok, R., Peralta-Ferriz, C., Alkire, M., Rigor, I., Andersen, R., Steele, M., 2012. Changing Arctic Ocean freshwater pathways. Nature 481, 66-70.

Nørgaard-Pedersen, N., Spielhagen, R.F., Erlenkeuser, H., Grootes, P.M., Heinemeier, J., Knies, J., 2003. Arctic Ocean during the Last Glacial Maximum: Atlantic and polar domains of surface water mass distribution and ice cover. Paleoceanography 18, 1063-1081.

Nørgaard-Pedersen, N., Spielhagen, R.F., Thiede, J., Kassens, H., 1998. Central Arctic surface ocean environment during the past 80,000 years. Paleoceanography 13, 193-204.

Not, C., Hillaire-Marcel, C., 2012. Enhanced sea-ice export from the Arctic during the Younger Dryas. Nat. Commun. 3, 647.

Peterson, B.J., Holmes, R.M., McClelland, J.W., Vörösmarty, C.J., Lammers, R.B., Shiklomanov, A.I., Shiklomanov, I.A., Rahmstorf, S., 2002. Increasing river discharge to the Arctic Ocean. Science 298, 2171-2173.

Phillips, R.L., Grantz, A., 2001. Regional variations in provenance and abundance of ice-rafted clasts in Arctic Ocean sediments: implications for the configuration of late Quaternary oceanic and atmospheric circulation in the Arctic. Mar. Geol. 172, 91-115.

Pin, C., Zalduegui, J.S., 1997. Sequential separation of light rare-earth elements, thorium and uranium by miniaturized extraction chromatography: Application to isotopic analyses of silicate rocks. Anal. Chim. Acta 339, 79-89.

Piotrowski, A.M., Banakar, V.K., Scrivner, A.E., Elderfield, H., Galy, A., Dennis, A., 2009. Indian Ocean circulation and productivity during the last glacial cycle. Earth Planet. Sci. Lett. 285, 179-189.

Polyak, L., Bischof, J., Ortiz, J.D., Darby, D.A., Channell, J.E.T., Xuan, C., Kaufman, D.S., Løvlie, R., Schneider, D.A., Eberl, D.D., Adler, R.E., Council, E.A., 2009. Late Quaternary stratigraphy and sedimentation patterns in the western Arctic Ocean. Global Planet. Change 68, 5-17.

Polyak, L., Curry, W.B., Darby, D.A., Bischof, J., Cronin, T.M., 2004. Contrasting glacial/interglacial regimes in the western Arctic Ocean as exemplified by a sedimentary record from the Mendeleev Ridge. Palaeogeogr. Palaeoclimatol. Palaeoecol. 203, 73-93.

Polyak, L., Jakobsson, M., 2011. Quaternary sedimentation in the Arctic Ocean: Recent advances and further challenges. Oceanography 24, 52-64.

Poore, R.Z., Osterman, L., Curry, W.B., Phillips, R.L., 1999. Late Pleistocene and Holocene meltwater events in the western Arctic Ocean. Geology 27, 759-762.

Porcelli, D., Andersson, P.S., Baskaran, M., Frank, M., Björk, G., Semiletov, I., 2009. The distribution of neodymium isotopes in Arctic Ocean basins. Geochim. Cosmochim. Acta 73, 2645-2659.

Reimer, P.J., Baillie, M.G.L., Bard, E., Bayliss, A., Beck, J.W., Blackwell, P.G., Ramsey, C.B., Buck, C.E., Burr, G.S., Edwards, R.L., 2009. IntCal09 and Marine09 radiocarbon age calibration curves, 0–50,000 years cal BP. Radiocarbon 51, 1111-1150.

Rella, S.F., Uchida, M., 2011. Sedimentary organic matter and carbonate variations in the Chukchi Borderland in association with ice sheet and ocean-atmosphere dynamics over the last 155 kyr. Biogeosciences 8, 3545-3553.

Rutberg, R.L., Hemming, S.R., Goldstein, S.L., 2000. Reduced North Atlantic Deep Water flux to the glacial Southern Ocean inferred from neodymium isotope ratios. Nature 405, 935-938.

Schlosser, P., Bönisch, G., Rhein, M., Bayer, R., 1991. Reduction of deepwater formation in the Greenland Sea during the 1980s: Evidence from tracer data. Science 251, 1054-1056.

Semiletov, I., Savelieva, N., Weller, G., Pipko, I., Pugach, S., Gukov, A.Y., Vasilevskaya, L., 2000. The dispersion of Siberian river flows into coastal waters: meteorological, hydrological and hydrochemical aspects. NATO Sci. Ser. 2 Environ. Secur. 70, 323-366.

Sharma, M., Basu, A.R., Nesterenko, G., 1992. Temporal Sr-, Nd- and Pb-isotopic variations in the Siberian flood basalts: Implications for the plume-source characteristics. Earth Planet. Sci. Lett. 113, 365-381.

Spielhagen, R.F., Baumann, K.-H., Erlenkeuser, H., Nowaczyk, N.R.N.R., Nørgaard-Pedersen, N., Vogt, C., Weiel, D., 2004. Arctic Ocean deep-sea record of northern Eurasian ice sheet history. Quat. Sci. Rev. 23, 1455-1483.

Spielhagen, R.F., Erlenkeuser, H., 1994. Stable oxygen and carbon isotopes in planktic foraminifers from Arctic Ocean surface sediments: Reflection of the low salinity surface water layer. Mar. Geol. 119, 227-250.

Spivack, A.J., Wasserburg, G.J., 1988. Neodymium isotopic composition of the Mediterranean outflow and the eastern North Atlantic. Geochim. Cosmochim. Acta 52, 2767-2773.

Stein, R., Matthiessen, J., Niessen, F., Krylov, A., Nam, S., Bazhenova, E., 2010. Towards a better (litho-) stratigraphy and reconstruction of Quaternary paleoenvironment in the Amerasian Basin (Arctic Ocean). Polarforschung 79, 97-121.

Stein, R., Nam, S.I.I., Schubert, C., Vogt, C., Futterer, D., Heinemeier, J., 1994. The last deglaciation event in the eastern central Arctic Ocean. Science 264, 692-696.

Stokes, C., Clark, C., Winsborrow, M., 2006. Subglacial bedform evidence for a major palaeo-ice stream and its retreat phases in Amundsen Gulf, Canadian Arctic Archipelago. J. Quat. Sci. 21, 399-412.

Stokes, C.R., Clark, C.D., 2003. Laurentide ice streaming on the Canadian Shield: A conflict with the soft-bedded ice stream paradigm? Geology 31, 347-350.

Stokes, C.R., Clark, C.D., Darby, D.A., Hodgson, D.A., 2005. Late Pleistocene ice export events into the Arctic Ocean from the M'Clure Strait Ice Stream, Canadian Arctic Archipelago. Global Planet. Change 49, 139-162.

Svendsen, J.I., Alexanderson, H., Astakhov, V.I., Demidov, I., Dowdeswell, J.A., Funder, S., Gataullin, V., Henriksen, M., Hjort, C., Houmark-Nielsen, M., Hubberten, H.W., Ingólfsson, Ó., Jakobsson, M., Kjær, K.H., Larsen, E., Lokrantz, H., Lunkka, J.P., Lysså, A., Mangerud, J., Matiouchkov, A., Murray, A., Möller, P., Niessen, F., Nikolskaya, O., Polyak, L., Saarnisto, M., Siegert, C., Siegert, M.J., Spielhagen, R.F., Stein, R., 2004. Late Quaternary ice sheet history of northern Eurasia. Quat. Sci. Rev. 23, 1229-1271.

Tachikawa, K., Jeandel, C., Roy-Barman, M., 1999. A new approach to the Nd residence time in the ocean: the role of atmospheric inputs. Earth Planet. Sci. Lett. 170, 433-446.

Tarasov, L., Peltier, W., 2005. Arctic freshwater forcing of the Younger Dryas cold reversal. Nature 435, 662-665.

Timmermans, M.L., Garrett, C., 2006. Evolution of the deep water in the Canadian Basin in the Arctic Ocean. J. Phys. Oceanogr. 36, 866-874.

Winsborrow, M., Clark, C.D., Stokes, C.R., 2004. Ice streams of the Laurentide ice sheet. Geogr. Phys. Quat. 58, 269-280.

Winter, B.L., Johnson, C.M., Clark, D.L., 1997. Strontium, neodymium, and lead isotope variations of authigenic and silicate sediment components from the Late Cenozoic Arctic Ocean: implications for sediment provenance and the source of trace metals in seawater. Geochim. Cosmochim. Acta 61, 4181-4200.

Woo, M.K., Thorne, R., 2003. Streamflow in the Mackenzie Basin, Canada. Arctic 56, 328-340.

Woodgate, R.A., Aagaard, K., Muench, R.D., Gunn, J., Björk, G., Rudels, B., Roach, A., Schauer, U., 2001. The Arctic Ocean boundary current along the Eurasian slope and the adjacent Lomonosov Ridge: Water mass properties, transports and transformations from moored instruments. Deep-Sea Res. Part I 48, 1757-1792.

Zimmermann, B., Porcelli, D., Frank, M., Andersson, P.S., Baskaran, M., Lee, D.-C., Halliday, A.N., 2009. Hafnium isotopes in Arctic Ocean water. Geochim. Cosmochim. Acta 73, 3218-3233.

Table 1. Line scan data[a] and IRD (> 2mm) counts[b] of PS72/410-1 (All data from Jang et al., *in preparation*)

Depth (cm)	L*	a*	Depth (cm)	IRD counts
0.5-1.5	36.17	3.72	0-1	5
1.5-2.5	35.87	3.94	1-2	3
2.5-3.5	34	4.34	2-3	3
3.5-4.5	36.64	3.92	3-4	2
4.5-5.5	41.24	2.72	4-5	2
5.5-6.5	40.92	2.62	5-6	1
6.5-7.5	39.41	3.53	6-7	4
7.5-8.5	37.77	3.89	7-8	2
8.5-9.5	40.23	3.17	8-9	3
9.5-10.5	42.03	3.06	9-10	2
10.5-11.5	41.67	3.2	10-11	2
11.5-12.5	41.09	3.88	11-12	1
12.5-13.5	42.05	4.01	12-13	2
13.5-14.5	40.59	4.05	13-14	11
14.5-15.5	37.74	4.96	14-15	1
15.5-16.5	34.03	5.08	15-16	1
16.5-17.5	33.25	5.01	16-17	0
17.5-18.5	33.96	4.85	17-18	0
18.5-19.5	34.63	4.76	18-19	0
19.5-20.5	39.6	3.64	19-20	0
20.5-21.5	38.43	4.26	20-21	0
21.5-22.5	40.63	4.16	21-22	0
22.5-23.5	43.49	3.37	22-23	0
23.5-24.5	45.37	3.27	23-24	0
24.5-25.5	42.96	3.68	24-25	1
25.5-26.5	41.89	4.19	25-26	0
26.5-27.5	40.86	3.88	26-27	1
27.5-28.5	42.11	3.62	27-28	5
28.5-29.5	43.53	3.11	28-29	2
29.5-30.5	42.72	3.5	29-30	0
30.5-31.5	36.47	4.29	30-31	0
31.5-32.5	37.82	4.62	31-32	1
32.5-33.5	36.33	4.8	32-33	4
33.5-34.5	37.36	4.75	33-34	17
34.5-35.5	37.7	4.56	34-35	3
35.5-36.5	36.65	4.93	35-36	4
36.5-37.5	39.51	4.37	36-37	2
-	-	-	37-38	1
-	-	-	38-39	0

[a]Line scan data of 38 cm long subcore were measured using the Avvatech digital imaging system. Output files are the Lightness L* (0% (black) to 100% (white)) and the red-green color space a* (negative (green) to positive (red).

[b]IRD (>2 mm) of box core were counted at 1 cm intervals across the x-ray slab. The number of IRD counts mean number of gravel size particles in 10 * 1 * 1 cm sediments.

Table 2. AMS ^{14}C ages of planktonic foraminifera *N. pachyderma* sin.

Sediment core	Depth (cm)	AMS ^{14}C ages (years)	1σ	Calibrated ages (years)[a]	1σ
PS72/410-1[b]	1-2	5,795	45	5,078	104
	10-11	18,100	120	19,842[*]	232
Jang et al. *in preparation*	13-14	27,450	300	30,768	238
	20-21	43,660	2,670	45,845	2,221
94B16 Poore et al. (1999)	2-3	4,680	50	3,591	72
	4-5	7,750	50	7,282	57
	6-7	10,050	50	9,755	99
	10-11	11,300	60	11,285	69
	13-14	12,250	60	12,720	81
	16-17	29,680	170	32,550	362
	17-18.5	41,250	850	43,846[*]	639
	19-20	31,930	280	35,006	237
	19.5-20.5	33,810	350	36,961	399
	20-21	36,610	480	40,306	636
	21-22	36,890	570	40,584	657
	23-24	37,770	580	41,406	461
	26-27	42,310	980	44,607	727
	33-34	49,500	2400	> 50,000[#]	-
HLY0503-8JPC Adler et al. (2009)	0-1	3,981	46	2,757	44
	3-4	8,530	25	7,983	31
	7-8	9,314	76	8,866[*]	115
	14-15	8,940	63	8,405	65
	24-25	9,917	50	9,575	61
	25-26	11,445	30	11,529	119
	32-33	36,250	730	39,882[*]	835
	34-35	32,480	470	35,651[*]	586
	43-44	38,660	980	42,005[*]	718
	48-49	30,950	400	34,115	472
	56-57	37,820	880	41,348	749
	62-63	40,500	1,300	43,344	927
PS2185 Nørgaard-Pedersen et al. (1998) & Spielhagen et al. (2004)	0-1	3,080	65	1,656	85
	1-2	3,505	65	2,171	89
	2-3	4,955	60	3,950	88
	4-5	5,690	60	4,925	76
	6-7	7,140	75	6,572	90
	7-8	8,375	75	7,837	79
	8-9	8,770	85	8,237	87
	9-10	10,710	85	10,575	94
	10-11	16,530	150	18,283[*]	257
	11-12	13,650	160	14,247	318
	12-13	15,960	110	17,708	182
	13-14	18,510	190	20,326	432
	14-15	19,970	290	22,108	372
	15-16	25,900	250	29,296	326
	16-17	30,780	530	33,919	582
	19-20	34,070	550	37,356	690

[a]The AMS ages were converted to calendar years using Marine09 (Reimer et al., 2009) with ΔR=1,000 (Hanslik et al., 2010).

[b]AMS ^{14}C ages were measured on planktonic foraminifera *N. pachyderma* sin. at Leibniz Lab., Kiel. All data from Jang et al., *in preparation*

[*,#]Not applicable due to contamination and calibration limitation.

Table 3. Neodymium isotope analysis results

Depth Interval (cm)	$^{143}Nd/^{144}Nd$[a]	ε_{Nd}[b]	2σ[c]
0~1	0.512093	-10.63	0.27
1~2	0.512118	-10.14	0.27
2~3	0.512109	-10.31	0.27
3~4	0.512113	-10.23	0.27
4~5	0.512096	-10.57	0.27
5~6	0.512102	-10.47	0.27
6~7	0.512114	-10.22	0.27
7~8	0.512122	-10.06	0.27
8~9	0.512082	-10.85	0.27
9~10	0.512074	-11.00	0.27
10~11	0.512047	-11.54	0.27
11~12	0.512102	-10.46	0.27
12~13	0.512073	-11.03	0.27
13~14	0.512052	-11.44	0.27
14~15	0.511999	-12.46	0.27
15~16	0.512031	-11.85	0.27
16~17	0.512046	-11.54	0.27
17~18	0.512104	-10.42	0.27
18~19	0.512129	-9.94	0.27
19~20	0.512156	-9.40	0.27
20~21	0.512175	-9.02	0.27
21~22	0.512163	-9.27	0.27
22~23	0.512159	-9.35	0.27
23~24	0.512153	-9.47	0.27
24~25	0.512186	-8.82	0.27
25~26	0.512195	-8.63	0.27
26~27	0.512167	-9.20	0.27
27~28	0.512148	-9.57	0.27
28~29	0.512131	-9.89	0.27
29~30	0.512130	-9.91	0.27
30~31	0.512129	-9.93	0.27
31~32	0.512123	-10.04	0.27
32~33	0.512137	-9.78	0.27
33~34	0.512136	-9.79	0.27
34~35	0.512145	-9.62	0.27
35~36	0.512120	-10.11	0.27
36~37	0.512118	-10.14	0.27
37~38	0.512103	-10.44	0.27
38~39	0.512100	-10.50	0.27

[a]All samples were analyzed using IsotopX IsoProbe-T TIMS and normalized by $^{143}Nd/^{144}Nd$ of average standard JNdi ratios (0.512100 ± 0.000015 (2σ), n=79).
[b]$\varepsilon_{Nd} = [(^{143}Nd/^{144}Nd)_{sample}/(^{143}Nd/^{144}Nd)_{CHUR} - 1] \times 10^4$, where $(^{143}Nd/^{144}Nd)_{CHUR}$ = 0.512638 (Jacobsen and Wasserburg, 1980).
[c]An external uncertainty of 0.27 ε_{Nd} (2σ) which is larger than internal 2 standard error were applied.

Table 4. Present-day ε_{Nd} values and Nd flux of Arctic rivers

River	ε_{Nd}	C_{Nd} (pM)[a]	Mean discharge (km^3/yr)	Nd flux[b]
Kolyma	-6.0 ± 0.4[c]	129[c]	74[e]	1.0
Lena	-13.6 ± 0.4[c]	477[c]	525[e]	26.2
Lena	-14.2 ± 0.3[d]	826[d]	525[e]	45.4
Yenisey	-5.2 ± 0.3[d]	154[d]	586[e]	9.5
Ob	-6.1 ± 0.3[d]	2152[d]	403[e]	90.9
Mackenzie	-12.9 ± 0.3[d]	111[d]	284[f]	3.3

[a]Uncertainty is less than 5%.
[b]The Nd fluxes were calculated by multiplying the Nd concentration by mean annual riverine discharge and normalized to Kolyma River.
[c]from Porcelli et al. (2009)
[d]Zimmermann et al. (2009)
[e]Semiletov et al. (2000)
[f]Woo and Thorne (2003)

Table 5. Neodymium isotope analysis results for ARA02B/03B

Depth Interval (cm)	$^{143}Nd/^{144}Nd$[a]	ε_{Nd}[b]	2σ[c]
0~0.5	0.512270	-7.17	0.34
0.5~1	0.512268	-7.21	0.34
1~2	0.512282	-6.95	0.34
2~3	0.512277	-7.04	0.34
9~10	0.512267	-7.24	0.34
15~16	0.512247	-7.62	0.34
17~18	0.512216	-8.23	0.60
19~20	0.512244	-7.68	0.34
21~22	0.512252	-7.52	0.34
24~25	0.512258	-7.41	0.34
25~26	0.512259	-7.38	0.34
27~28	0.512242	-7.72	0.34
28~29	0.512173	-9.07	0.43
30~31	0.512213	-8.30	0.34
31~32	0.512204	-8.46	0.65
32~33	0.512206	-8.43	0.34
35~36	0.512181	-8.91	0.45

[a]All samples were analyzed using IsotopX IsoProbe-T TIMS and normalized by $^{143}Nd/^{144}Nd$ of average standard JNdi-1 ratios (0.512100 ± 0.000015 (2σ), n=79).

[b]$\varepsilon_{Nd} = [(^{143}Nd/^{144}Nd)_{sample}/(^{143}Nd/^{144}Nd)_{CHUR} - 1] \times 10^4$, where $(^{143}Nd/^{144}Nd)_{CHUR}$ = 0.512638 (Jacobsen and Wasserburg, 1980).

[c]An external uncertainty of 0.34 ε_{Nd} (2σ) is generally reported. When internal standard errors are larger than 0.34 ε_{Nd}, internal 2 standard error were applied.

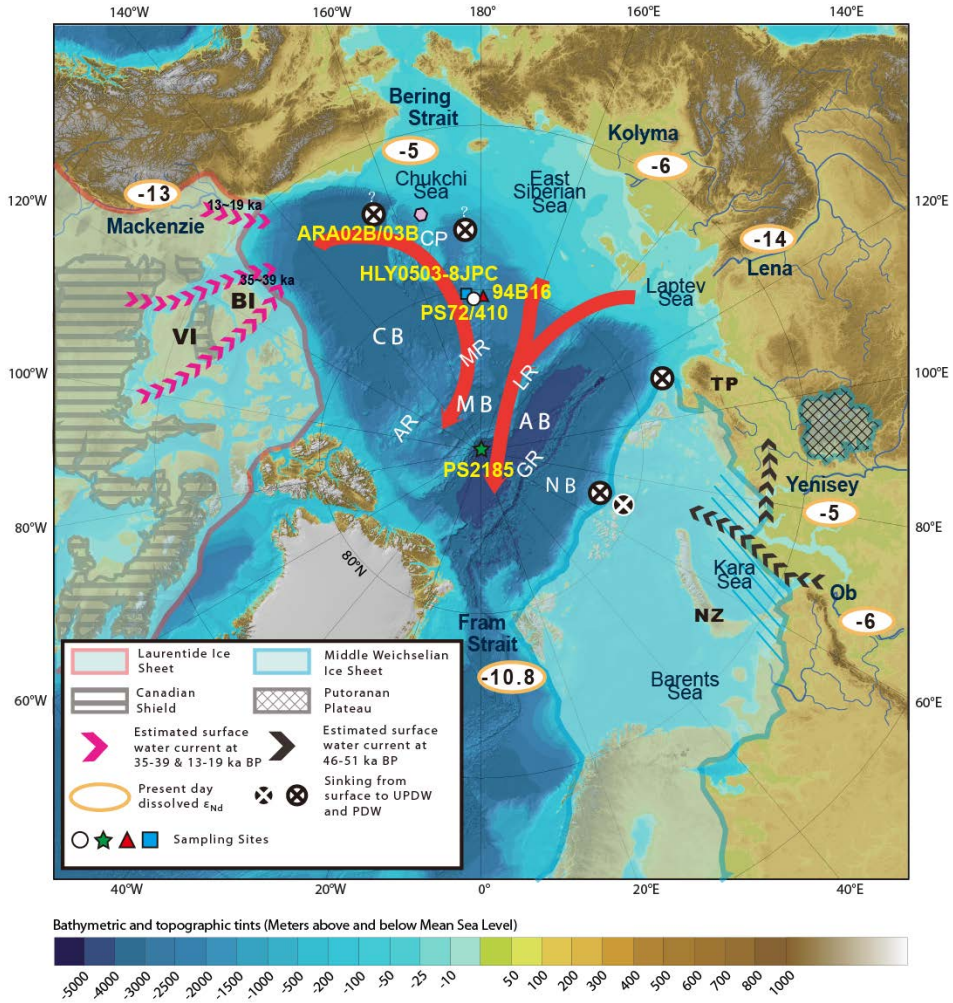

Figure 1. Schematic map of the circum-Arctic showing core sites, ocean circulation and glacial ice sheet distributions. Red arrows mark the Beaufort Gyre and the Transpolar Drift in the Arctic Ocean. The sediment core site ARA02B/03B (pink hexagon) on the Chukchi Plateau, site PS72/410 (open circle) and neighboring cores 94B16 (red triangle; Poore et al., 1999) and HLY0503-8JPC (blue square; Adler et al., 2009) on the Mendeleev Ridge and core PS2185 (green star; Haley et al., 2007) on the Lomonosov Ridge are marked. The ε_{Nd} values of major inflows into the Arctic Ocean are given inside orange circles (Porcelli et al., 2009 and references therein). The Laurentide Ice Sheet margin during full glacial condition (red line) and the Middle Weichselian Ice Sheet margin at 60 ka BP (blue line) are simplified from Stokes and Clark (2003) and Svendsen et al. (2004), respectively. Note that the Putorana Plateau was under ice during the Middle Weichselian glaciation. Estimated surface water currents during different periods are shown in purple and dark gray arrows. CB : Canada Basin, MB : Makarov Basin, AB : Amundsen Basin, NB : Nansen Basin, CP : Chukchi Plateau, MR : Mendeleev Ridge, AR : Alpha Ridge, GR : Gakkel Ridge, VI : Victoria Island, BI : Banks Island, TP : Taimyr Peninsula, NZ : Novaya Zemlya . The base map is from Jakobsson et al. (2012).

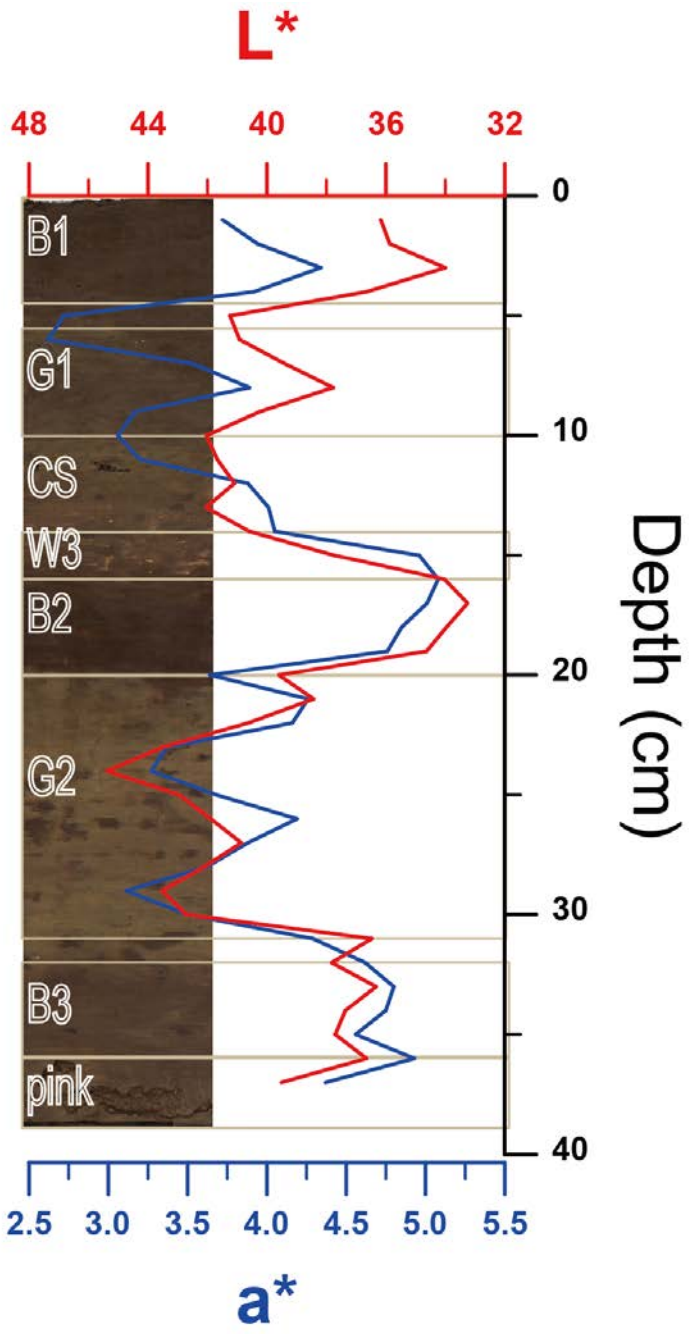

Figure 2. Classification of sediment layers based on the x-radiograph and L* and a* values. Brown layers have determined by relatively low L* and high a* values while the marks of gray layer have determined based on the shipboard data (the sediment sizes and colors distinguished between 10-11 cm and 5.5-10 cm, there were also some white spots at 11-14 cm, Jokat, 2008) and x-radiograph. The accurate position of W3 and pinkish dolomite spot were questionable due to widely scattered spots observed in the x-radiograph. CS stands for condensed section. All data from Jang et al., *in preparation*

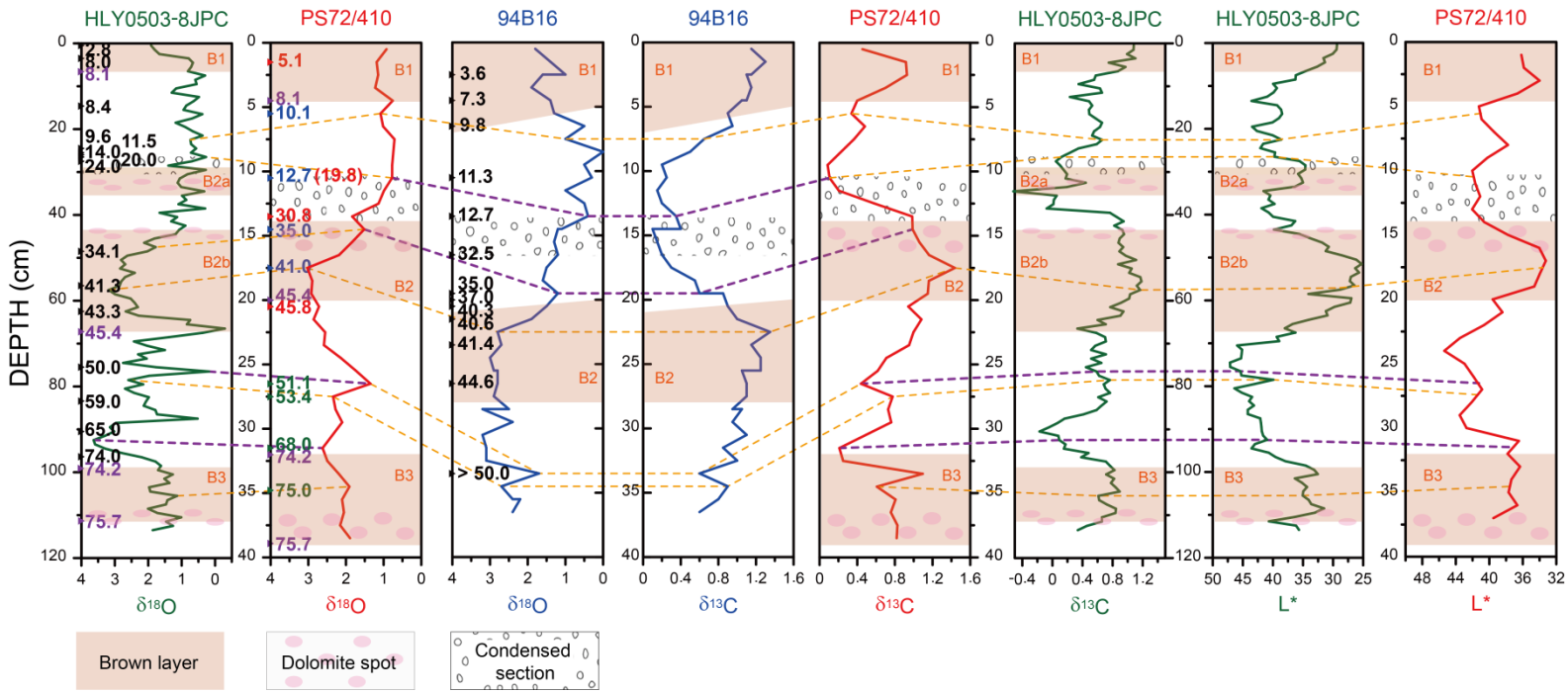

Figure 3. Age model construction for core PS72/410-1 using AMS ^{14}C ages (ka BP, n=4, red numbers) and by correlating δ^{18}O, δ^{13}C, and L* (red lines) with neighboring cores 94B16 (blue lines) and HLY0503-8JPC (green lines) for which stratigraphic ages have already been constructed (Adler et al., 2009; Poore et al., 1999). The numbers (ka BP) in the δ^{18}O graph of PS72/410-1 represent AMS ^{14}C ages (red), correlation ages with core 94B16 (blue) and core HLY0503-8JPC (green), and stratigraphic ages (purple). The numbers (ka BP) in the δ^{18}O graph of 94B16 and HLY0503-8JPC indicate AMS ^{14}C ages (ka BP). Purple dashed lines link the the age control points and orange dashed lines mark other tie points. Characteristic sediment layers are shown with patterned rectangles. AMS ^{14}C ages, δ^{18}O, δ^{13}C, and L* values for PS72/410-1 from Jang et al., *in preparation*

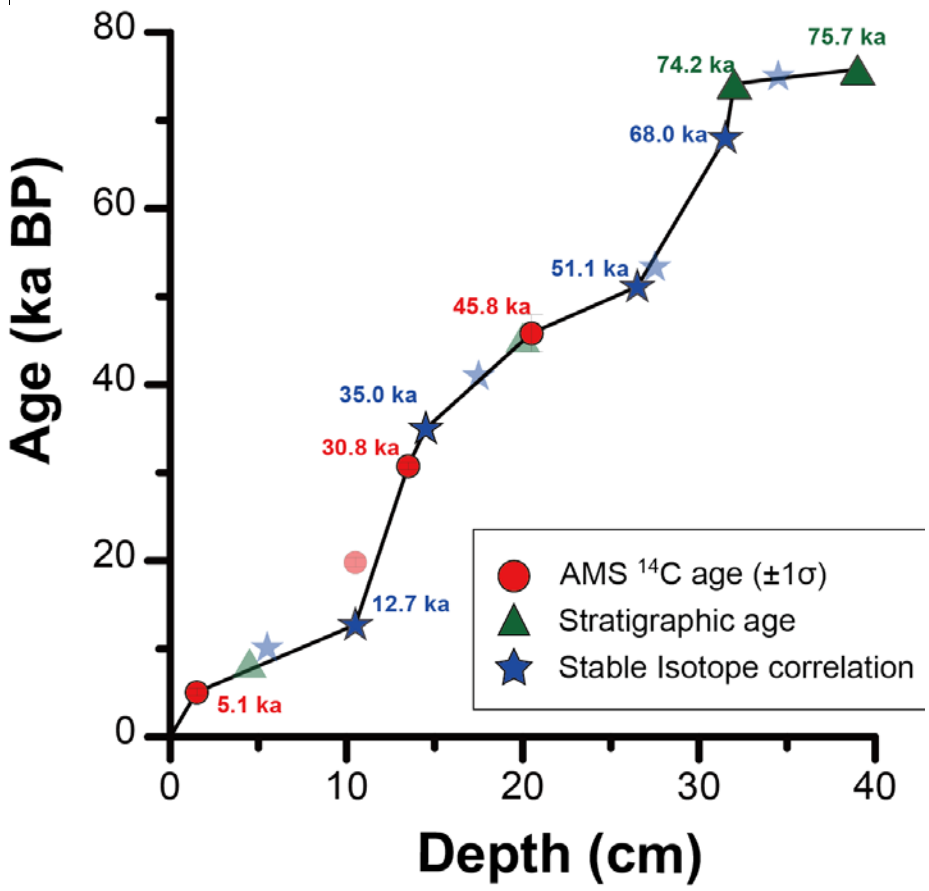

Figure 4. The age model of core PS72/410-1. Symbols with black outlines indicate age control points including the three AMS ^{14}C ages, two stratigraphic ages, and four stable isotope correlation ages. Symbols without outlines represent stable isotope and L*, stratigraphic tie points and contaminated AMS ^{14}C age.

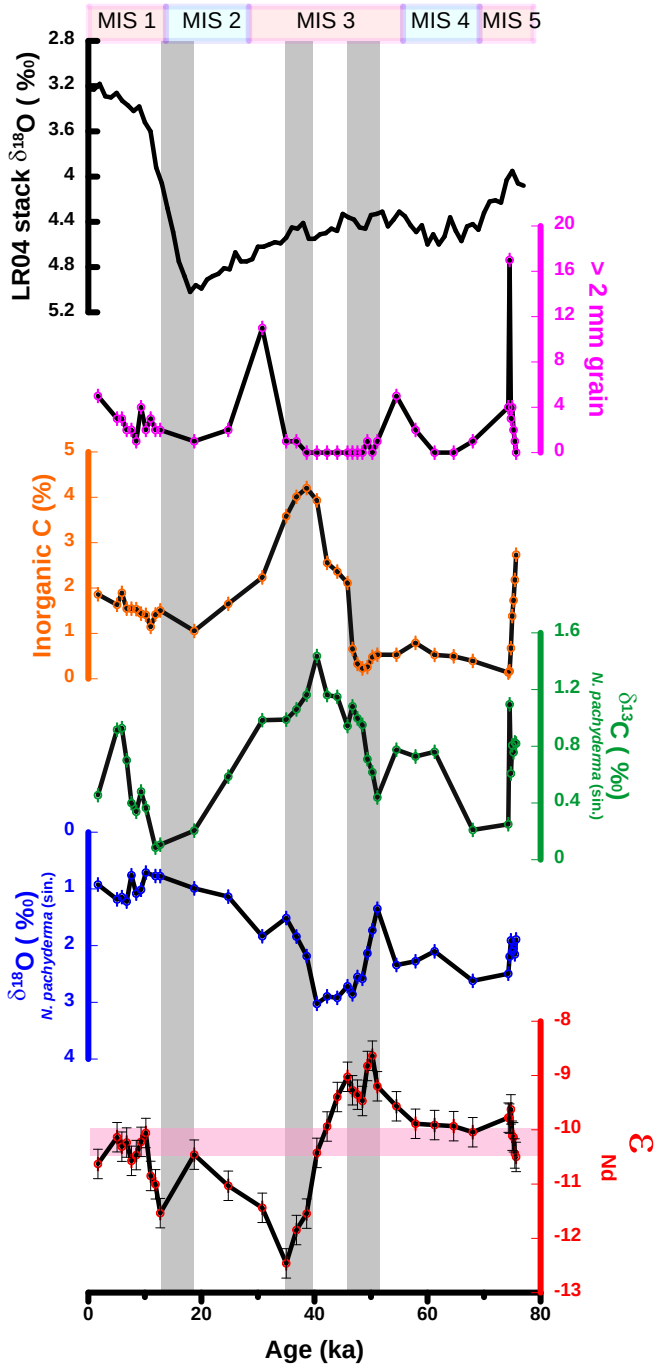

Figure 5. Geochemical data of core PS72/410-1. Three prominent ε_{Nd} deviations (grey shading) from the average (pink shading) are compared with the variation in other proxies. Coarse-grained IRD count, bulk carbonate content, and $\delta^{18}O$ and $\delta^{13}C$ of planktonic foraminifera (*N. pachyderma* sin.) are shown (data from Jang et al., *in preparation*). LR04 stack $\delta^{18}O$ values are from Lisiecki and Raymo (2005).

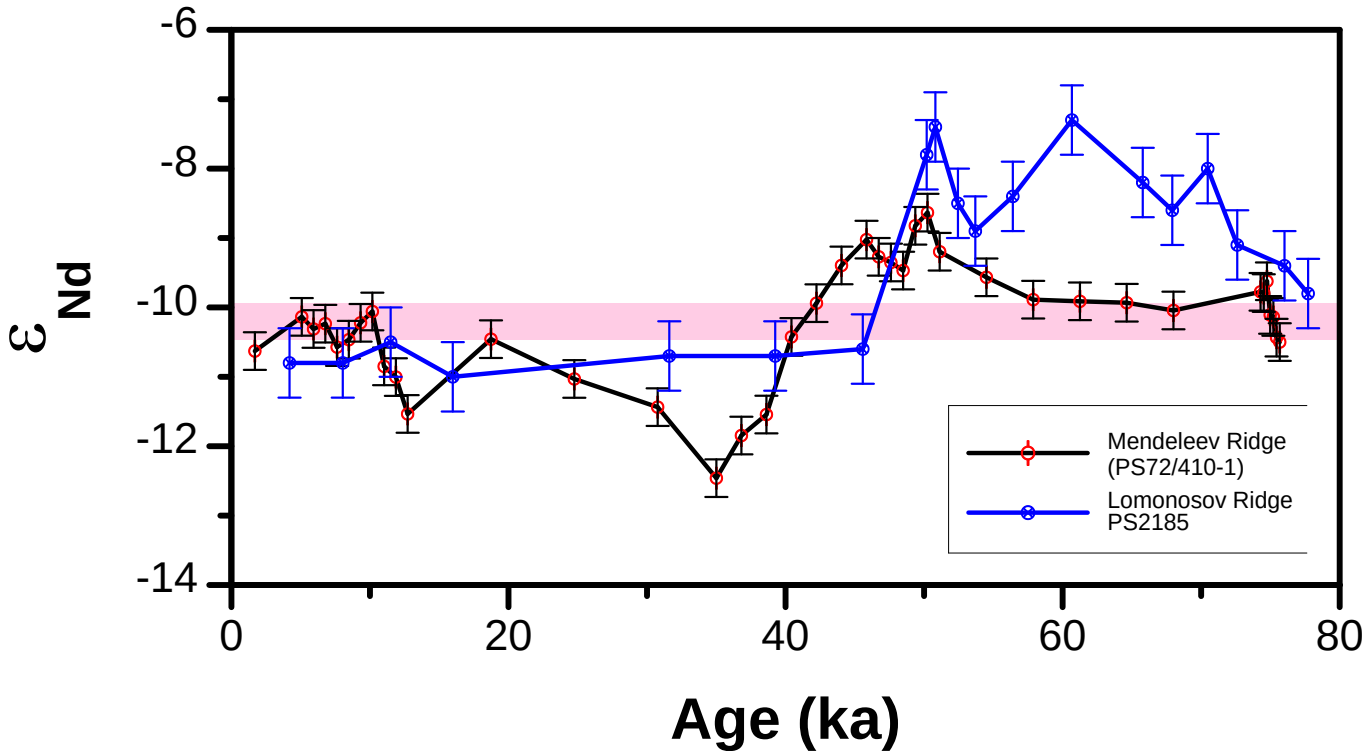

Figure 6. Authigenic ε_{Nd} records in the Arctic Ocean. $\varepsilon_{Nd} = [(^{143}Nd/^{144}Nd)_{sample}/(^{143}Nd/^{144}Nd)_{CHUR} - 1] \times 10^4$. Red circles are for the Polar Deep Water on the Canada Basin side of the Mendeleev Ridge, and blue circles represent the Upper Polar Deep Water on the Amundsen Basin side of the Lomonosov Ridge (Haley et al., 2007). Error bars indicate ± 2 external uncertainties (0.27 ε_{Nd} units in PS72/410-1 and 0.5 ε_{Nd} units in PS2185).

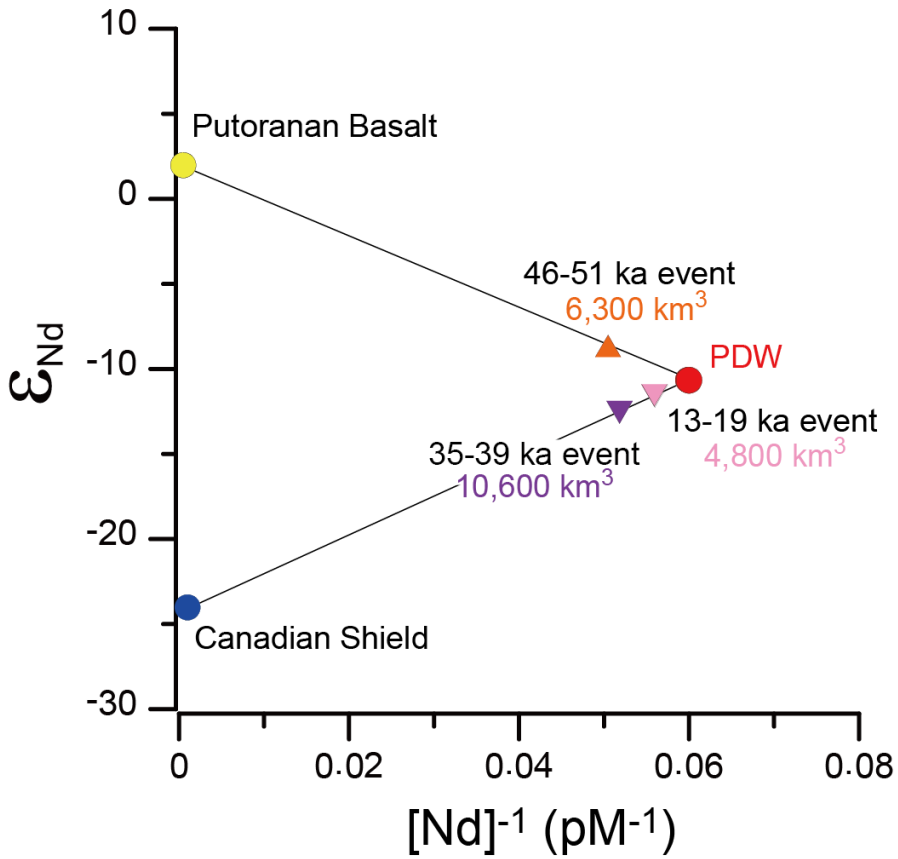

Figure 7. Neodymium mixing diagram showing the three end members. Yellow circle marks the Putoranan basalt sourced freshwater ([Nd] = 2,000 pM; ε_{Nd} = +2 from Sharma et al. (1992)). The blue circle represents the Canadian Shield sourced freshwater ([Nd] = 1,000 pM; ε_{Nd} = -24 from Winter et al. (1997)). The red circle is for the present-day PDW ([Nd] = 16.7 pM from Porcelli et al. (2009), ε_{Nd} = -10.63). Freshwater added to the PDW of the western Arctic Ocean are 6,300 km^3 at 46-51 ka BP (orange triangle), 10,600 km^3 at 35-39 ka BP (purple triangle) and 4,800 km^3 at ~13 ka BP (pink triangle).

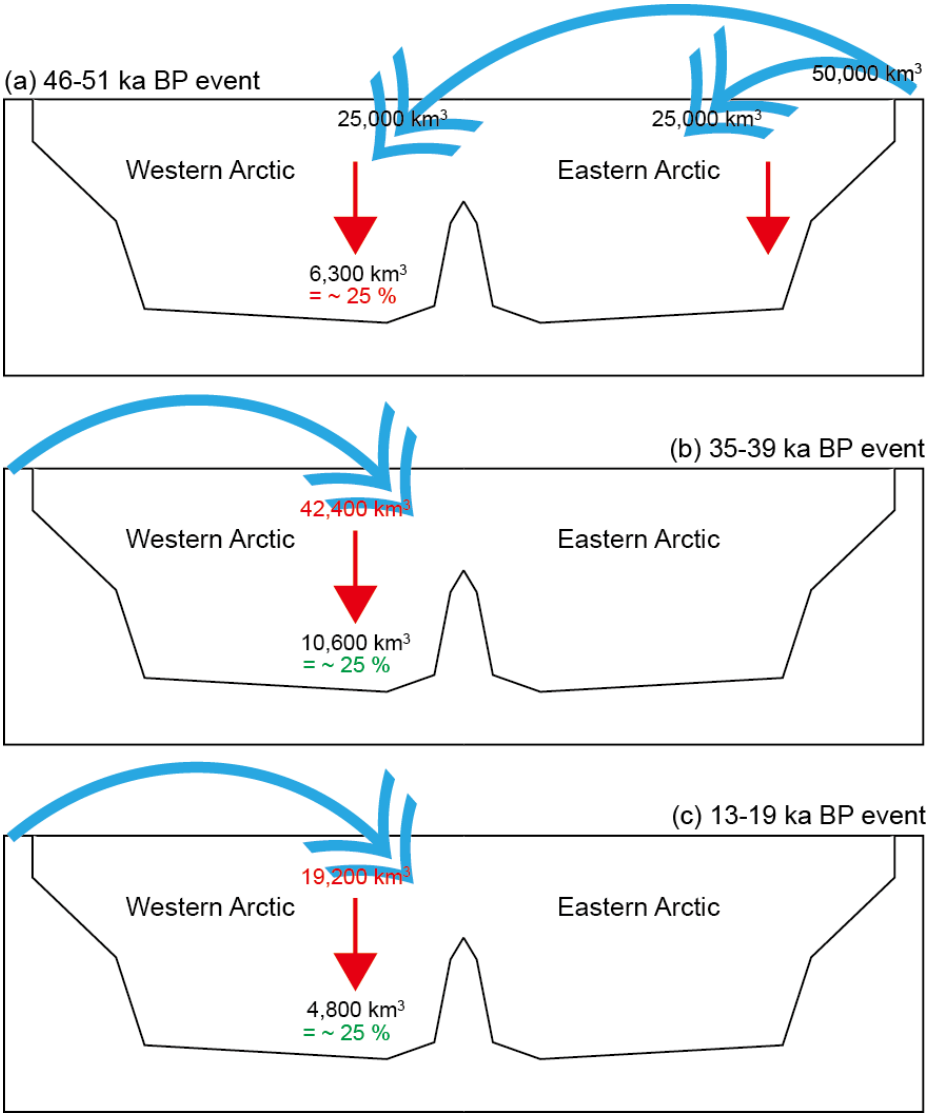

Figure 8. Schematic illustration of three freshwater discharge events with estimated their volumes. (a) 46-51 ka BP, (b) 35-39 ka BP, and (c) 13-19 ka BP freshwater discharge events.

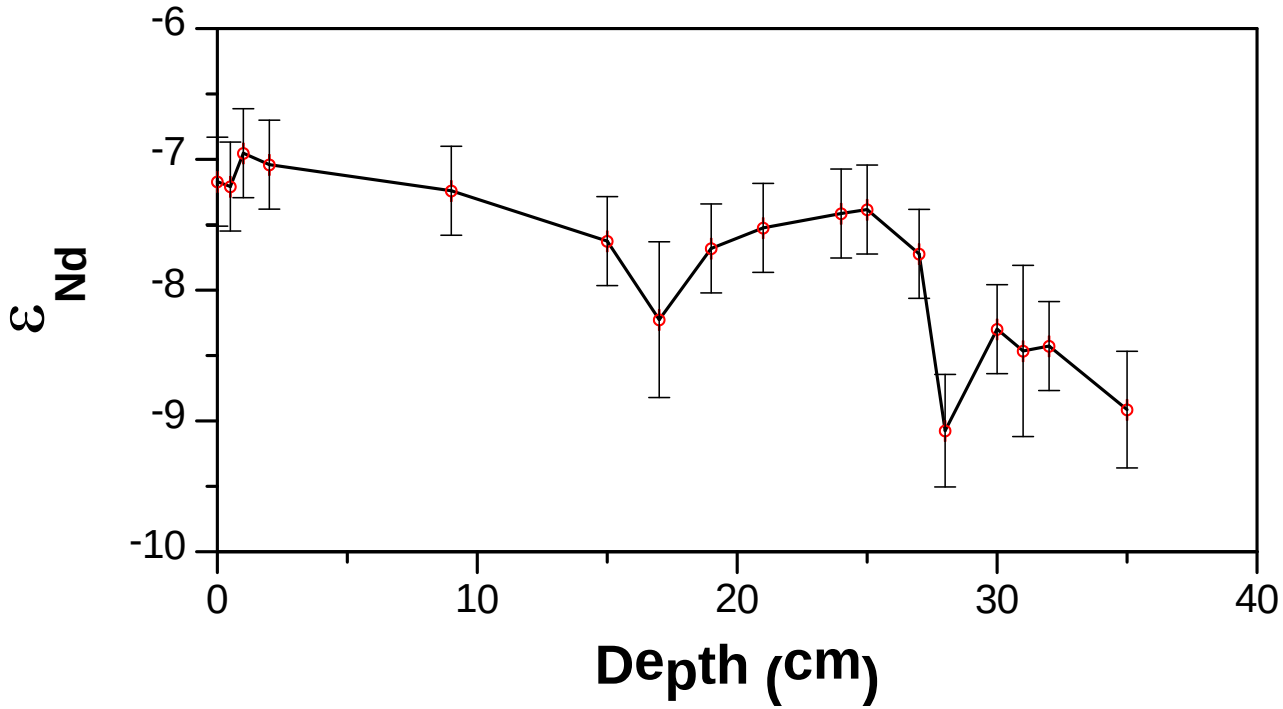

Figure 9. Authigenic ε_{Nd} records in the Arctic Ocean. $\varepsilon_{Nd} = [(^{143}Nd/^{144}Nd)_{sample}/(^{143}Nd/^{144}Nd)_{CHUR} - 1] \times 10^4$. Red circles are for the AL on the Chukchi Plateau. Error bars indicate $\pm 2\sigma$ external uncertainties (0.34 ε_{Nd} units) in PS72/410-1. When internal standard errors (2se) are larger than 2σ, then the errors are reported as 2se

국 문 초 록

북태평양과 북대서양의 통로에 위치하는 북극해는 전지구적 기후시스템에 중요한 역할을 한다고 알려져 있다. 이는, 북태평양 해수를 비롯하여, 전 지구 강물량의 10%에 달하는 여러 강물, 그리고 얼음이 녹아 형성되는 담수를 포함하는 북극해로 유입되는 다양한 근원의 수괴들과 관련되어 있다. 이들은 북극해의 염도를 낮추고, 북대서양으로 흘러가 북대서양 심층수의 형성에 영향을 주며 전 지구적 열 분배에 영향을 끼치기 때문이다. 본 저자는, 서북극해의 멘델레예프 해령과 척치 플라토의 자생성 네오디뮴 동위원소를 고해상도로 분석하여, 과거 46,000~51,000년, 35,000~39,000년, 그리고 13,000~19,000년 전에 서북극해로 유입되는 막대한 양의 담수가 발생했음을 재현하였으며, 홀로세 후기 기간 동안 태평양 해수의 유입이 증가하였음을 복원하였다. 46,000~51,000년전, 상대적으로 높은 네오디뮴 동위원소 값이 관찰되었다. 이는, 중기 바이크셀리안 빙하기 동안 확장된 바렌츠-카라 빙상에 의해 경로가 차단된 막대한 양의 아이스댐 호수가 많은 양의 레디오제닉한 네오디뮴을 동반하며, 북극해로 유입되었을 것으로 추정된다. 당시, 동북극해의 반시계방향의 표층수 흐름은 오늘날에 비해 강했을 것으로 추정된다. 반면, 35,000~39,000년, 13,000~19,000년 전에는 상대적으로 낮은 네오디뮴이 관찰되는데, 이는 로렌티드 빙상으로부터 유입된 막대한 양의 담수가 대륙붕

지역에 축적된 언레디오제닉 네오디뮴을 쓸고 들어가며 나타난 결과로 여겨진다. 이 때, 서북극에 발달한 시계방향의 표층수 흐름은 오늘날과 같거나 동북극해 방향으로 확장했을 것으로 보인다. 매스밸런스 계산에 의하면, 네오디뮴 동위원소의 변화를 일으키는 담수의 양이 오래된 이벤트부터 6,300, 10,600, 그리고 4,800 km^3에 달함을 나타내며, 이로 유추할 수 있는 당시 북극해로 유입되는 막대한 양의 담수가 북대서양 심층수의 형성에도 영향을 끼칠 수 있음을 시사한다. 홀로세 후기기간에는 코어의 하층에서 상층으로 이동함에 따라, 네오디뮴 동위원소 값의 증가가 관찰된다. 이는 해수면의 증가에 따라, 북극해로 유입되는 북태평양 해수의 유량이 증가하며 발생된 결과로 보인다. 두 차례의, 네오디뮴 동위원소 값의 하강은, 얼음의 용해에 의한 언레디오제닉 담수의 유입 혹은 얼음 형성에 의한 북태평양 해수의 유입 감소로 해석될 수 있지만, 연대모델의 불확실성과 지화학적 정보의 결여로 인해 가설의 검증은 보류되었다.

주요어 : 네오디뮴 동위원소, 서북극해, 북태평양, 표층수, 담수, 고기후
학 번 : 2010-23138

Acknowledgment